Series magnetic coupled reactor saturation considerations for high voltage AC and DC power systems

Heidary, Amir; Ghaffarian Niasar, Mohamad; Popov, Marjan

DOI
10.1016/j.ijepes.2024.109909

Publication date
2024

Document Version
Final published version

Published in
International Journal of Electrical Power & Energy Systems

Citation (APA)
Heidary, A., Ghaffarian Niasar, M., & Popov, M. (2024). Series magnetic coupled reactor saturation considerations for high voltage AC and DC power systems. *International Journal of Electrical Power & Energy Systems*, *158*, Article 109909. https://doi.org/10.1016/j.ijepes.2024.109909

Electrical Power and Energy Systems 158 (2024) 109909

Contents lists available at ScienceDirect

International Journal of Electrical Power and Energy Systems

journal homepage: www.elsevier.com/locate/ijepes

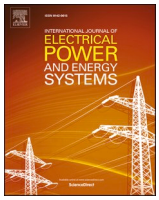

Series magnetic coupled reactor saturation considerations for high voltage AC and DC power systems

Amir Heidary *, Mohamad Ghaffarian Niasar, Marjan Popov

Delft University of Technology, Faculty of EEMCS, Mekelweg 4, 2628CD Delft, The Netherlands

ARTICLE INFO

Keywords:
Fault current limiter
Series reactor
Saturation region

ABSTRACT

The rapid increase of integrated distributed generators results in higher fault currents in the future modern grids. A remedy for the concern is employing series reactors as fault current limiters. This paper elaborates on a ferromagnetic core series reactor, which, when saturated, adversely affects the operation of the series reactor during faults. The main goal of the paper is to calculate grid and series reactor coefficients by applying a simplified power line model during a fault condition. These coefficients are the primary considerations of a series reactor design to avoid its saturation. Moreover, the study of the relationship between the reactor inductance and obtained coefficients will be carried out. The obtained results are validated by simulations performed in MATLAB Simulink.

1. Introduction

Series reactors (SRs) are protection devices that impose series impedance during fault conditions [1] to limit the fault current magnitude or overvoltage [2] and protect vulnerable power system equipment [3]. Series current limiting reactors have been widely investigated for the protection of both AC power systems [4] and DC power systems [5]. Moreover, its effects have also been investigated for the point of common coupling voltage restoration in the power grid [6]. To provide acceptable series impedance, SR must avoid saturation [7].

In most of the recently studied magnetic core SRs employed as fault current limiters (FCL), insufficient attention has been given to the vital issue of core saturation during the fault limiting mode [8].

The paper deals with the determination of the two coefficients that cause the SR to operate out of the saturation region. Moreover, the mentioned coefficients are calculated for different voltage levels for both HVAC and HVDC systems. Finally, the inductance of the SR, by taking into account the calculated coefficients, will be analyzed and investigated through MATLAB Simulink simulation.

2. Saturation considerations of the SR for AC systems

The analytical study is conducted for a single-line power system in which a line-to-ground fault occurs, as illustrated in Fig. 1. In this system, V_{th} is the Thevenin RMS voltage, I_f is the fault current, R_{th}, and L_{th} are the Thevenin resistance and inductance computed for the observed system. L_{SR} is the inductance of the SR, R_f is the fault resistance, and ω is the grid frequency.

Power systems can be exposed to different high- or low-impedance fault currents. Considering that SR saturation is mostly possible for low-impedance faults, the analysis is conducted for the highest possible fault current. The steady-state analysis is employed to extract the faulty system coefficients and SR considerations as follows:

$$Z_f = (R_{th} + R_f) + j\omega(L_{th} + L_{SR}) \tag{1}$$

By applying the following assumptions:

$$\omega(L_{th} + L_{SR}) \gg R_{th} + R_f, \quad L_{SR} \gg L_{th} \tag{2}$$

The faulty system impedance in Fig. 1 is expressed as:

$$|Z_f| = \omega L_{SR} \tag{3}$$

Consequently, the fault current is calculated as:

$$I_f = V_{th}/\omega L_{SR} \tag{4}$$

Considering the magnetic flux of SR φ_{SR} in Fig. 2, the linking flux equation is written as in (6) by assuming (5).

$$\varphi_{SR} = \varphi_m, \quad \varphi_m \gg \varphi_l \tag{5}$$

* Corresponding author.
E-mail address: a.heidary@tudelft.nl (A. Heidary).

https://doi.org/10.1016/j.ijepes.2024.109909
Received 18 September 2023; Received in revised form 7 February 2024; Accepted 28 February 2024
Available online 8 March 2024

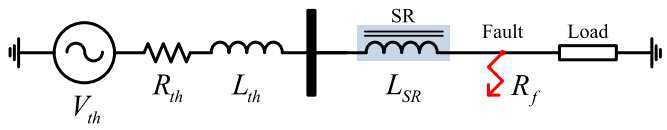

Fig. 1. Single-line diagram of the studied power system (line-to-ground fault occurrence).

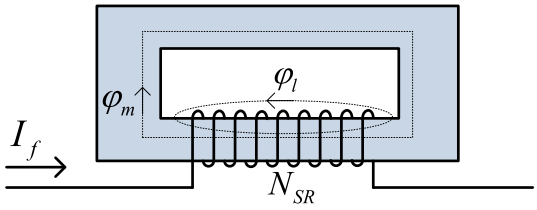

Fig. 2. Magnetic flux in SR.

$$\varphi_{SR} = \frac{L_{SR}.I_f}{N_{SR}} \tag{6}$$

Eq. (6) claims that the value of the magnetic flux φ_m (series reactor main linking flux φ_{SR}) is much higher than that of the leakage flux φ_l. By applying (4)–(6), the following can be derived:

$$\varphi_{SR} = \frac{V_{th}}{\omega}.\frac{1}{N_{SR}} \tag{7}$$

$$B_{SR} = \frac{(V_{th}/\omega)}{(N_{SR}.A_{SR})} \tag{8}$$

Here N_{SR} and A_{SR} are the numbers of winding turns and the SR core cross-section, respectively. Furthermore, B_{SR} introduces the magnetic flux density of the SR.

There are two coefficients in (8). One of them is G_c, as shown in (9), which introduces the coefficient depending on the grid specifications and is called a grid coefficient, and SR coefficient R_c, which we denote as the reactor coefficient expressed by (10).

$$G_c = V_{th}/\omega \tag{9}$$

$$R_c = N_{SR}.A_{SR} \tag{10}$$

Fig. 3 depicts an illustration of a B-I characteristic for an SR. Magnetic flux density should be selected before the nonlinear and saturation region is reached, and based on that, the R_c coefficient of SR can be determined (the selected flux density can be varied based on the physics of the SR core). At the same time, the grid coefficient depends on system voltage and angular frequency.

Therefore, boundary equations (11) and (12) can be used to calculate the coefficients for different grids as listed in Table 1.

$$B_{SR} = \frac{G_c}{R_c} \leqslant 1.4T \tag{11}$$

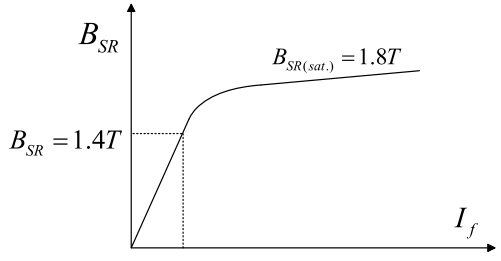

Fig. 3. Magnetic flux in SR and selected example of the magnetic flux density.

Table 1
Coefficient calculations for different AC power grid.

Grid voltage	G_c ($\omega = 314$)	R_c ($\omega = 314$)	G_c ($\omega = 377$)	R_c ($\omega = 377$)
63 kV	200	<143	167	<119
120 kV	382	<273	318	<227
200 kV	636	<454	531	<379
400 kV	1274	<910	1061	<758

$$R_c \geqslant G_c/1.4 \tag{12}$$

Considering the grid and SR coefficient, an AC SR can be designed out of the saturation region to protect the HVAC system. In addition, assuming that the SR limiter does not limit fault current overshot, the overshot factor can multiply in G_c, and then the SR coefficient is recalculated.

3. Saturation considerations of the SR in the DC system

Focusing on the specifications and coefficients of DC systems and DC SR, the simple faulty DC system is considered, as depicted in Fig. 4.

The first assumption is shown by (13), where the considered fault is a low impedance fault, and the SR inductance is much higher than the system's Thevenin inductance L_{th}.

$$R_{th} \gg R_f, \quad L_{SR} \gg L_{th} \tag{13}$$

In the HVDC system, the nature of the fault current is expressed by the Neperian equation [9], and the DC circuit breaker (DCCB) operates approximately in the linear parts of the fault current curve. Moreover, in reality, this current follows its rising trend until the DCCB operation. The operation time of the DCCB is very fast (between 2 and 4 ms). Therefore, during this period, the linear Eq. (14) can be fitted to the fault current of the DC system with a very close match. This region is shown in Fig. 5, where after fault occurrence, the current increases almost linearly toward its maximum fault current. However, it will be interrupted by DCCB in 2 ms.

By taking into account the operation time of the DCCB, the fault current in SR is the linear term of the curve, and by considering some approximation, the equation of the SR current during this period is expressed by (14) and (15).

$$i_f(t) = \alpha t \tag{14}$$

$$\alpha = \frac{V_{th}/R_{th}}{L_{SR}/R_{th}} = \frac{V_{th}}{L_{SR}} \tag{15}$$

In (14), the fault current is a function of time t linearly. This equation consists of the current linear rate of rise α which can be calculated by (15). Eq. (15) is considered by the division of the maximum current value (V_{th}/R_{th}) and time constant of the R-L circuit (L_{SR}/R_{th}), assuming fault occurred at $t = 0$. In (16), t_{CB} is the corresponding time of the DCCB operation. In the conducted analysis, this time is considered to be 2 or 4 ms. Moreover, the steady-state current is assumed to be much lower than the fault current.

$$I_f = \frac{V_{th}.t_{CB}}{L_{SR}} \tag{16}$$

In (16), I_f is the HVDC system fault current once the DCCB opens the faulty line. By applying (16) in (6), Eqs. (17) and (18) can be written as follows:

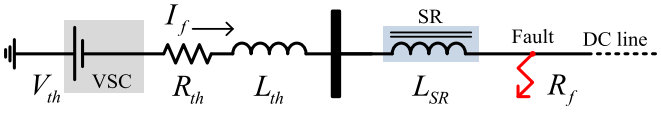

Fig. 4. DC system diagram in fault condition.

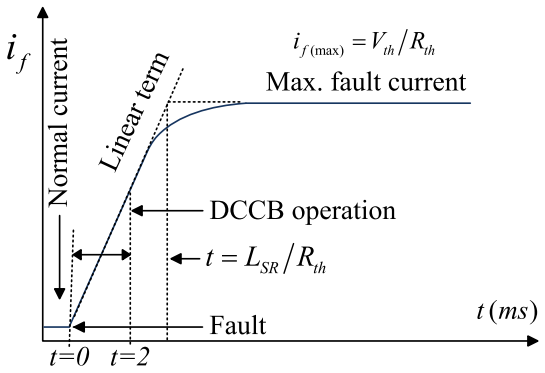

Fig. 5. DC system normal and fault current.

$$\varphi_{SR} = \frac{V_{th}.t_{CB}}{N_{SR}} \tag{17}$$

$$B_{SR} = \frac{(V_{th}.t_{CB})}{(N_{SR}.A_{SR})} \tag{18}$$

As a result of the obtained equation, the grid coefficient G_c and SR coefficient R_c for the HVDC system can be written as follows:

$$G_c = V_{th}.t_{CB} \tag{19}$$

$$R_c = N_{SR}.A_{SR} \tag{20}$$

Table 2 shows computed coefficients by considering different levels of the HVDC voltage using Eqs. (19) and (20).

Considering the calculated coefficient for both HVAC and HVDC systems, the SR winding turns and core cross-section can be obtained to avoid SR saturation using Tables 1 and 2. The next section discusses some concerns and limitations on how to design ferromagnetic core SRs.

The important factors for SR design considering core saturation are illustrated in Fig. 6. Although important, thermal and insulation matters are not discussed because these factors almost have no effects on the saturation issue. From a magnetic point of view, four factors, namely core cross-section, the number of winding turns, core effective length, and core material, affect the SR's behavior. Among these factors, only core cross-section A_{SR} and winding turn N_{SR}, which affects SR saturation, can be seen in (10), (11), (18), and (19), while all four factors are used to calculate the inductance of the SR.

The relationship between grid coefficient G_c, SR coefficient R_c, and the inductance of SR, L_{SR}, provide a clear insight into the possibility of designing the SR to protect the power system against fault currents. In Fig. 7(a) and (b), R_c is shown for different G_c, and are presented for both AC and DC reactors by implementing the saturation boundary of the SR. The area under the curve is the saturation region of SR, and the area above the curve is the out-of-saturation region. The assumed condition is that $\omega = 314$, and the operation time of DCCB is 2 ms. To avoid SR saturation for the highest possible fault current, a point above the plotted boundary should be obtained for each G_c.

Fig. 8 presents a 3D line plot for the inductance of the SR as a function of the SR coefficient boundary as defined by (10) and (20). To calculate the inductance of the SR shown by (21), the core permeability and core length proportion are expressed by (22), which is taken from in-practice core specifications. In addition, the R_c here is assumed to be 143, as shown in Table 1.

Table 2
Coefficient calculations for different DC power grid.

Grid voltage	G_c ($t = 2$ ms)	R_c ($t = 2$ ms)	G_c ($t = 4$ ms)	R_c ($t = 4$ ms)
200 kV	400	<286	800	<571
400 kV	800	<571	1600	<1143
800 kV	1600	<1143	2400	<1714

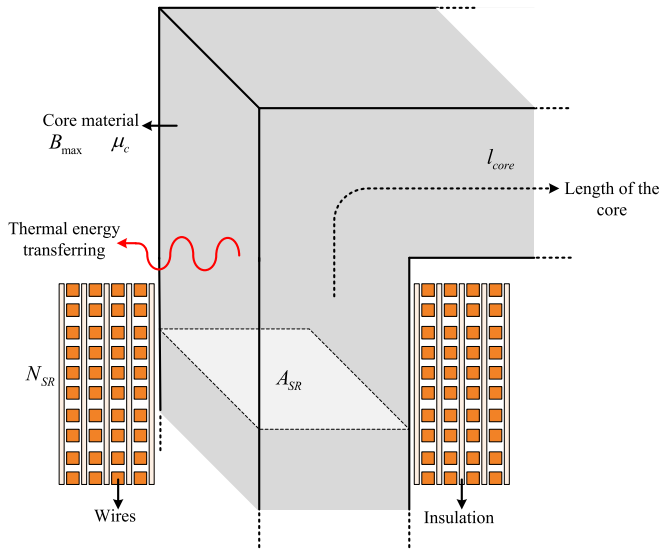

Fig 6. Magnetic parameters of the magnetically coupled SR.

$$L_{SR} = \frac{A_{SR}.N_{SR}.\mu_c}{l_{core}} \tag{21}$$

$$\mu_c/l_{core} = 0.0017 \tag{22}$$

In this curve, it is obtained that the minimum inductance of the SR is 34H for the core cross-section of 1 m^2, and the number of winding turns is 143. The trend of the curve shows that for a lower value of the inductance, it is necessary to enlarge the core cross-section to a very high value and reduce the number of SR winding turns. This scenario results in the design of an extra-large SR to avoid saturation. Instead of the explained scenario, when the value of the core cross-section is decreased while the number of winding turns is increased, the reactor core size can be reasonable. However, in this way, the inductance of SR is very high, the insulation between turns is a concern, and SR is not easy to control. Both scenarios prove that by taking into account the saturation, both the size and inductance of the SR will be extremely large, which makes the design of magnetically coupled SR very difficult.

Furthermore, if the designers ignore the SR coefficient, the designed SR will surely go into saturation in case of low impedance faults.

To clarify the inductance of the SR as a function of R_c, three points of the curve are listed in Table 3.

4. Conclusion

This paper discusses the saturation concerns of the series reactors as protection devices. Two coefficients are introduced that clearly show the saturation limitations of the series reactors. The result is that the series reactor saturation will be avoided by only considering the grid coefficient (G_c) and by balancing the series reactor winding turns as well as core cross-section as the series reactor coefficient (R_c). By considering these coefficients, it is shown that to avoid SR saturation, the inductance and the size of the series reactor ferromagnetic core or the winding turns for both high-voltage DC and AC grids have to be extremely large, which makes it impractical to construct and implement in the gird.

CRediT authorship contribution statement

Amir Heidary: Writing – original draft, Software, Formal analysis, Data curation. **Mohamad Ghaffarian Niasar:** Writing – review & editing, Supervision, Methodology, Investigation. **Marjan Popov:** Writing – review & editing, Validation, Supervision, Methodology.

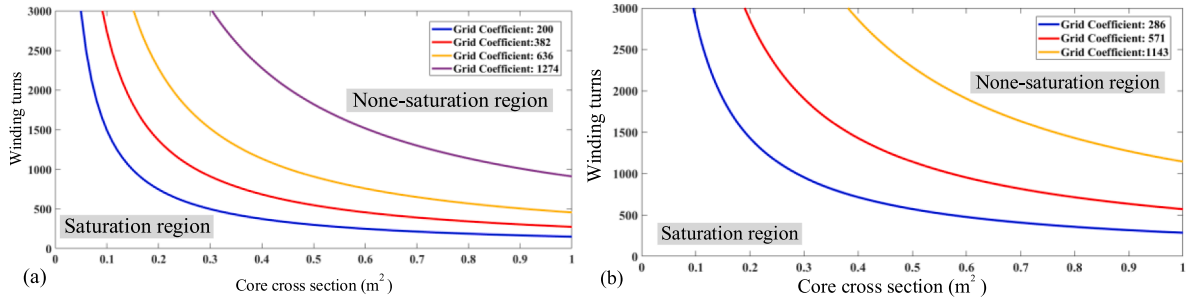

Fig. 7. SR saturation boundary a) AC SR, b) DC SR.

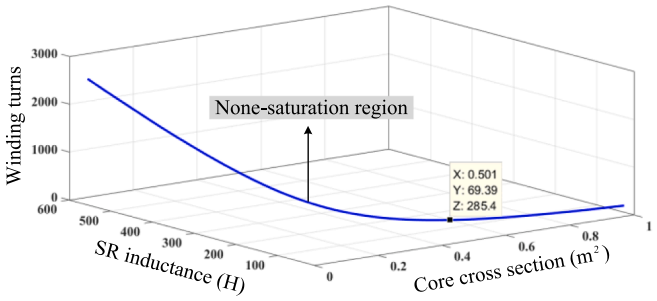

Fig. 8. The plot of the SR inductance function of the SR coefficient.

Table 3
Inductance of SR function of R_C.

R_c	N_{SR} (turn)	A_{SR} (m^2)	L_{SR} (H)
143	143	1	34
143	286	0.5	69
143	2460	0.06	600

Declaration of competing interest

The authors declare that they have no known competing financial interests or personal relationships that could have appeared to influence the work reported in this paper.

Data availability

Data will be made available on request.

Acknowledgments

This research work has been financially supported by the Dutch Research Council, Nederlandse Organisatie voor Wetenschappelijk Onderzoek (NWO) through the research project No. 18699, “Protection of Future Power System Crucial Components”.

References

[1] Heidary A, Radmanesh H, Rouzbehi K, Mehrizi-Sani A, Gharehpetian GB. Inductive fault current limiters: a review. Electr Pow Syst Res 2020;187:106499.
[2] Korobeynikov SM, Krivosheev SI, Magazinov SG, Loman VA, Ya N. Suppression of incoming high-frequency overvoltage in transformer coils. IEEE Trans Power Delivery 2021;36(5):2988–94.
[3] Wang S, Zhou J, Shu J, Ma J, Qin K, Liu T. A bidirectional active DC fault current limiter based on coupled inductor. IEEE Trans Power Delivery 2022;37(5):4427–37.
[4] Kang BI, Park JD. Application of thyristor-controlled series reactor for fault current limitation and power system stability enhancement. Int J Electr Power Energy Syst 2014;63:236–45.
[5] Kartijkolaie HS, Radmehr M, Firouzi M. LVRT capability enhancement of DFIG-based wind farms by using capacitive DC reactor-type fault current limiter. Int J Electr Power Energy Syst 2018;102:287–95.
[6] Firouzi M, Gharehpetian GB, Pishvaei M. A dual-functional bridge type FCL to restore PCC voltage. Int J Electr Power Energy Syst 2013;46:49–55.
[7] Heidary A, Popov M, Moghim A, Niasar MG, Lekić A. The principles of controlled DC reactor fault current limiter for battery energy storage protection. IEEE Trans Ind Electron 2023;71(2):1525–34.
[8] Naphade V, Ghate V, Dhole G. Experimental analysis of saturated core fault current limiter performance at different fault inception angles with varying DC bias. Int J Electr Power Energy Syst 2021;130:106943.
[9] Heidary A, Radmanesh H, Rouzbehi K, Pou J. A DC-reactor-based solid-state fault current limiter for HVdc applications. IEEE Trans Power Delivery 2019;34(2):720–8.